A Tetranuclear Niobium Oxo Acetate Complex. Synthesis, X-ray Crystal Structure, and Characterization by Solid-State and Liquid-State NMR Spectroscopy

Nathalie Steunou, Christian Bonhomme, and Clément Sanchez*

Chimie de la Matière Condensée, UMR CNRS 7574, Université Pierre et Marie Curie, 75252 Paris, France

Jacqueline Vaissermann

Chimie des Métaux de transition, Université Pierre et Marie Curie, 75252 Paris, France

Liliane G. Hubert-Pfalzgraf

Chimie Moléculaire, Université de Nice−Sophia Antipolis, Parc Valrose, 06108 Nice Cedex 2, France

Received August 13, 1997

The compound $Nb_4O_4(OAc)_4(OPr^i)_8$ synthesized by reacting $Nb(OPr^i)_5$ and acetic acid has been fully characterized by single-crystal X-ray diffraction (a = 11,634(5) Å, b = 14,370(6)Å, c = 16,380(6) Å, α = 79.90(4)°, β = 71.78(4)°, γ = 79.21(4)°, triclinic, $P\bar{1}$, Z = 2) and multinuclear NMR experiments performed in the solid state and in solution. A simple possible mechanism that can account for its formation is presented. ^{13}C CP MAS experiments, using the IRCP sequence (inversion recovery cross polarization), are used to perform straightforward assignments of the resonances of the different isopropoxy ligands bonded to niobum. ^{17}O, ^{13}C, and ^{1}H NMR spectroscopies show that the cluster structure is fully preserved in solution.

Introduction

Increasing interest has been devoted to the study of transition metal oxo alkoxo clusters whose general formula is $M_xO_y(OR)_z$ (M = Ti, Zr, Nb).[1−4] These metallo-organic compounds play an important role in understanding and characterizing mixed transition metal oxo based materials prepared by sol−gel chemistry.[5−7] The sol−gel process is based on hydrolysis and condensation reactions of organometallic precursors of general formula $M(OR)_n$. The macromolecular metal−oxo-based networks thereby developed are predominantly amorphous and polydisperse, and the scarceness of structural data makes their characterization particularly difficult. They can be characterized using spectroscopic techniques,[8−10] which can provide accurate information about the structure of the oxo polymers by comparing them to well-calibrated defined references compounds such as crystalline metal oxo based complexes. In most cases, such metallo-organic complexes are obtained for small hydrolysis ratios. Numerous metal oxo alkoxide clusters (metal = Ti^{IV}, Zr^{IV}, Ce^{IV}) synthesized through hydrolysis and condensations reactions, with or without the presence of a complexing ligand, have received much attention and have been structurally characterized.[1−3, 11−14]

In contrast, much less work have been devoted to niobium oxo alkoxide complexes. $Nb_8O_{10}(OEt)_{20}$ was first obtained through controlled hydrolysis of niobium ethoxide, and its structure was resolved by single-crystal X-ray diffraction.[15] Another chemical route based on condensation of $NbO(OEt)_3$ with the release of two ether molecules Et_2O was proposed for the synthesis of the same octamer $Nb_8O_{10}(OEt)_{20}$.[16] Another approach which consists of generating water in situ through esterification reactions was used to produce various hexanuclear

(1) Day, V. W.; Eberspacher, T. A.; Klemperer, W. G.; Park, C. W. *J. Am. Chem. Soc.* **1993**, *115*, 8469.
(2) Toledano, P.; In, M.; Sanchez, C. *C. R. Acad. Sci Paris Ser. 2* **1991**, *313*, 1247.
(3) Sanchez, C.; In, M.; Toledano, P.; Griesmar, P. *Mater. Res. Soc. Symp. Proc.* **1992**, *271*, 669.
(4) Kickelbick, G.; Schubert, U. *Chem. Ber.* **1997**, *130*, 473.
(5) Campana, C. F.; Chen, Y.; Day, V. W.; Klemperer, W. G.; Sparks, R. A. *J. Chem. Soc., Dalton Trans.* **1996**, 691.
(6) Chen, Y. W.; Klemperer, W. G.; Park, C. W. *Mater. Res. Soc. Symp. Proc.* **1992**, *271*, 57.
(7) Sanchez, C.; Ribot, F. *New J. Chem.* **1994**, *1*, 1007.
(8) Blanchard, J.; Barboux-Doeuff, S.; Maquet, J.; Sanchez, C. *New J. Chem.* **1995**, *19*, 929.
(9) Day, V. W.; Eberspacher, T. A.; Klemperer, W. G.; Park, C. W.; Rosenberg, F. S. In *Chemical Processing of Advanced Materials*; Hench, L. L., West, K., Eds.; Wiley & Sons: New York; 1992; Chapter 2, p 257.
(10) Bastow, T. J.; Smith, M. E.; Whitfield, H. J. *J. Mater. Chem.* **1992**, *2*, 989.
(11) Day, V. W.; Eberspacher, T. A.; Klemperer, W. G.; Park, C. W.; Rosenberg, F. S. *J. Am. Chem. Soc.* **1991**, *113*, 8190.
(12) Day, V. W.; Eberspacher , T. A.; Chen, Y.; Hao, J.; Klemperer, W. G. *Inorg. Chim. Acta* **1995**, *229*, 391.
(13) Schmidt, R.; Mosset, A.; Galy, J. *J. Chem. Soc., Dalton Trans.* **1991**, *8*, 1999.
(14) Toledano, P.; Ribot, F.; Sanchez, C. *C. R. Acad. Sci Paris, Ser. 2* **1990**, *311*, 1315.
(15) Bradley, D. C.; Hurthouse, M. B.; Rodesiler, P. F. *Chem. Commun.* **1968**, *18*, 1112.
(16) Kessler, V. G.; Turova, N. Y.; Yanovskii, A. I.; Belokon, A. I.; Struchov, Y. T. *Russ. J. Inorg. Chem.* **1991**, *36*, 938.

S0020-1669(97)01024-0 CCC: $15.00
Published on Web 02/10/1998

complexes of titanium.[17−20] However, only one tetranuclear niobium cluster capped by four methacrylate ligands $Nb_4O_4(OMc)_4(OPr^i)_8$ (Mc = $O_2CCMeCH_2$, Pr^i = $CH(CH_3)_2$) was recently obtained using a similar approach.[21]

In this paper, we report a complete study of the $Nb_4O_4(OAc)_4(OPr^i)_8$ compound together with a possible mechanism for its formation. The structure is resolved by single-crystal X-ray diffraction. A full spectroscopic characterization in solution and in the solid state is presented (^{17}O, ^{13}C, and ^{1}H NMR spectrocopy in solution and ^{13}C solid-state NMR including magic-angle spinning and cross polarization (CP MAS)). The IRCP sequence (inversion recovery cross polarization) based on the standard CP experiment is used mainly to investigate local motion of the CH groups.

Results and Discussion

X-ray Structure Determination of $Nb_4O_4(OAc)_4(OPr^i)_8$ (1). The molecular structure of compound **1** was determined by single-crystal X-ray diffraction. A CAMERON[22] drawing and a polyhedral representation are shown in Figures 1 and 2, respectively. Fractional coordinates for the non-hydrogen atoms as well as selected bond distances and angles are given in Tables 1−3, respectively. Compound **1** is a centrosymmetric tetrameric cluster of formula $Nb_4O_4(OAc)_4(OPr^i)_8$ whose structure is similar to that already reported for the compound $Nb_4O_4(OMc)_4(OPr^i)_8$ (Mc = $O_2CCMeCH_2$).[21] The main feature of the crystal is the presence of two similar half-molecules in the asymmetric unit. The complex can be described as two Nb_2O_2 units linked by two corners corresponding to oxygen O(5) (or O(16)). Each unit contains two niobium octahedra sharing corners corresponding to oxygen O(6) (or O(11)). Each cluster contains four niobium atoms coordinated by two doubly bridging (μ_2-O) oxygens, two bridging acetate groups, and two terminal isopropoxy groups.

Niobium atoms are located in oxygen-distorted octahedra as was clearly observed with the niobium oxo based clusters $Nb_4O_4(OMc)_4(OPr^i)_8$ and $Nb_8O_{10}(OEt)_{20}$.[16,21]

Each octahedron exhibits Nb−O bonds ranging from 1.81(1) to 2.19(1) Å for the first molecule (and from 1.84(1) to 2.20(1) Å for the second one). In both clusters, there is a large dispersion of cis O−Nb−O bond angles (from 80.0(5) to 99.6(6)° for the first molecule and from 79.7(5) to 100.6(5)° for the second one) and trans O−Nb−O bond angles (from 156.2(5) to 176.3(5)° for the first molecule and from 157.9(5) to 178.0(6)° for the second one). The coordination of the bridging acetate group is quite symmetrical since the Nb−O bonds vary from 2.16(1) to 2.19(1)° for the first entity (and from 2.13(1) to 2.20(1)° for the second one). Each Nb−O bond of bridging acetate ligand is located in the trans position of short bonds, engaging the oxygen atoms μ_2-O or the oxygen atoms of isopropoxy groups. This can be explained by a π transfer either from the oxygen atoms of the terminal isopropoxy groups or from the oxygen atoms μ_2-O to the d orbitals of niobium atoms.

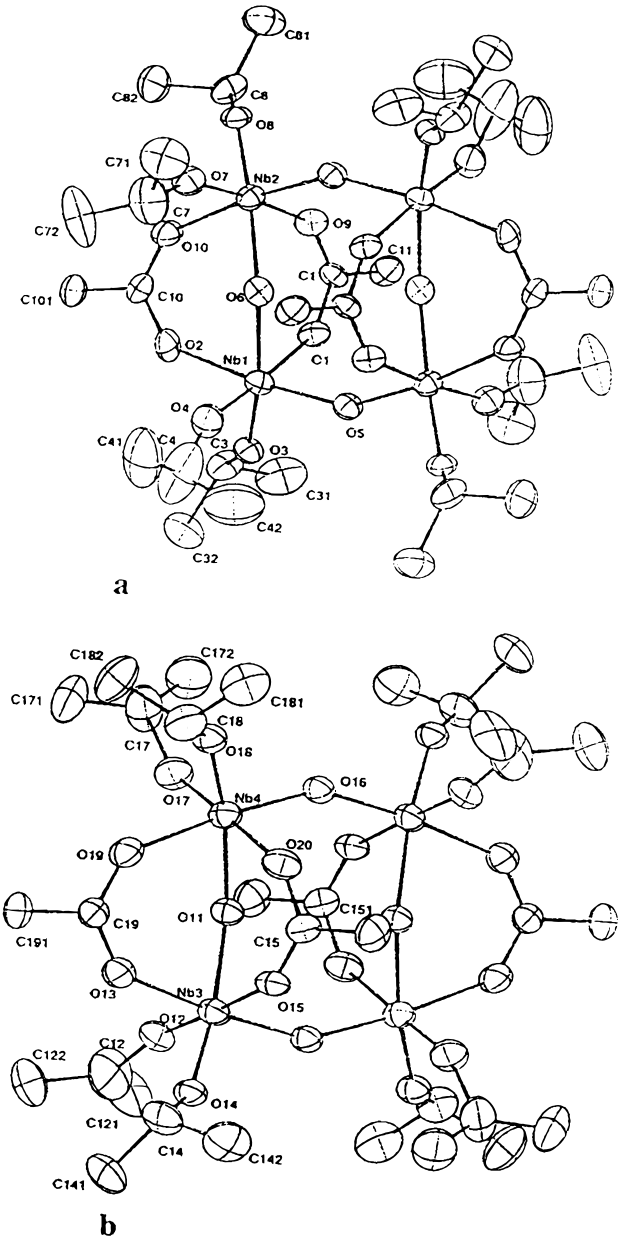

Figure 1. CAMERON drawing of the structure of compound **1**, showing 20% probability displacement ellipsoids. Two molecules, a and b, are represented. The asymmetric unit corresponds to two-half molecules.

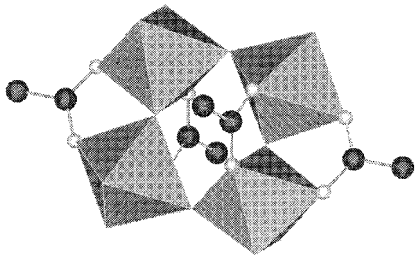

Figure 2. Polyhedral representation of compound **1**. The molecule corresponding to Nb(1) and Nb(2) is represented.

Isopropoxy groups can be distinguished by the anisotropic displacement parameter. This factor reflects the molecular motion. Each niobium atom is surrounded by two terminal isopropoxy groups which have different mobilities. For example, the carbon C(3) of the isopropoxy group linked to Nb(1) (U_{eq} = 0.082 Å^2) exhibits less mobility than the carbon C(4)

(17) Doeuff, S.; Dromzee, Y.; Taulelle, F.; Sanchez, C. *Inorg. Chem.* **1989**, *28*, 4439.
(18) Schubert, U.; Arpac, E.; Glaubitt, W.; Helmerich, A.; Chau, C. *Chem. Mater.* **1992**, *4*, 291.
(19) Gautier-Luneau, I.; Mosset, A.; Galy, J. *Z. Kristallogr.* **1987**, *180*, 83.
(20) Laaziz, I.; Larbot, A.; Guizard, C.; Durand, J.; Cot, L.; Joffre, J. *Acta Crystallogr.* **1990**, *C46*, 2332.
(21) Hubert-Pfalzgraf, L. G.; Abada, V.; Halut, S., Roziere, J. *Polyhedron* **1996**, *1*, 1.
(22) Watkin, D. J.; Prout, C. K.; Pearce, L. J. *CAMERON*; Chemical Crystallography Laboratory, University of Oxford: Oxford, U.K., 1996.

Table 1. Fractional Atomic Coordinates and Equivalent Isotropic Displacement Parameters (Å^2)

	x	*y*	*z*	U_{eq}[a]
		First Molecule		
Nb(1)	0.6582(2)	0.5739(1)	0.5379(1)	0.0728
Nb(2)	0.3313(2)	0.5615(1)	0.6347(1)	0.0744
O(1)	0.629(1)	0.4379(8)	0.6195(7)	0.0761
O(2)	0.595(1)	0.6306(9)	0.6628(8)	0.0853
O(3)	0.800(1)	0.5508(9)	0.5671(8)	0.0799
O(4)	0.676(1)	0.694(1)	0.4742(9)	0.1116
O(5)	0.706(1)	0.5032(9)	0.4407(7)	0.0786
O(6)	0.486(1)	0.5832(8)	0.5576(7)	0.0781
O(7)	0.252(1)	0.684(1)	0.6070(9)	0.0958
O(8)	0.213(1)	0.5242(9)	0.7390(8)	0.0809
O(9)	0.432(1)	0.4289(9)	0.6752(7)	0.0788
O(10)	0.400(1)	0.615(1)	0.7228(9)	0.0931
C(1)	0.541(2)	0.393(1)	0.659(1)	0.0671
C(3)	0.850(2)	0.531(2)	0.637(1)	0.0820
C(4)	0.741(5)	0.762(2)	0.422(3)	0.1480
C(7)	0.251(4)	0.774(2)	0.564(2)	0.1655
C(8)	0.195(2)	0.474(2)	0.828(1)	0.0963
C(10)	0.495(2)	0.644(1)	0.722(1)	0.0802
C(11)	0.573(2)	0.290(1)	0.685(1)	0.0979
C(31)	0.906(3)	0.432(3)	0.647(2)	0.1526
C(32)	0.952(2)	0.589(2)	0.623(2)	0.1065
C(41)	0.681(5)	0.841(3)	0.402(3)	0.2255
C(42)	0.790(4)	0.737(4)	0.336(3)	0.2409
C(71)	0.153(3)	0.796(2)	0.517(2)	0.1550
C(72)	0.268(4)	0.843(2)	0.611(2)	0.1788
C(81)	0.085(2)	0.420(2)	0.850(2)	0.1403
C(82)	0.174(3)	0.547(2)	0.889(2)	0.1430
C(101)	0.498(2)	0.693(2)	0.793(1)	0.0993
		Second Molecule		
Nb(3)	0.3717(2)	0.8635(1)	1.0238(1)	0.0846
Nb(4)	0.3605(2)	1.0608(1)	1.1410(1)	0.0849
O(11)	0.365(1)	0.9890(8)	1.0526(7)	0.0790
O(12)	0.251(1)	0.893(1)	0.9697(9)	0.1106
O(13)	0.238(1)	0.846(1)	1.151(1)	0.1079
O(14)	0.372(1)	0.7312(9)	1.0395(8)	0.0941
O(15)	0.502(1)	0.8245(8)	1.0953(8)	0.0837
O(16)	0.492(1)	1.1235(8)	1.0764(7)	0.0844
O(17)	0.237(1)	1.1598(9)	1.121(1)	0.1123
O(18)	0.352(1)	1.0848(9)	1.2532(8)	0.0965
O(19)	0.231(1)	0.968(1)	1.2199(9)	0.1065
O(20)	0.500(1)	0.943(1)	1.1674(9)	0.1009
C(12)	0.165(3)	0.879(3)	0.937(3)	0.1988
C(14)	0.361(3)	0.647(2)	1.102(2)	0.1120
C(15)	0.550(2)	0.870(1)	1.128(1)	0.0796
C(17)	0.167(3)	1.246(2)	1.148(3)	0.1554
C(18)	0.343(3)	1.040(2)	1.341(2)	0.1185
C(19)	0.191(2)	0.897(2)	1.209(2)	0.0938
C(121)	0.166(3)	0.918(3)	0.853(2)	0.1406
C(122)	0.049(3)	0.834(3)	1.006(3)	0.2006
C(141)	0.274(3)	0.593(2)	1.086(2)	0.1492
C(142)	0.488(3)	0.593(2)	1.095(2)	0.1567
C(151)	0.682(2)	0.839(2)	1.128(2)	0.1220
C(171)	0.052(3)	1.233(2)	1.209(2)	0.1715
C(172)	0.211(3)	1.324(2)	1.096(3)	0.1717
C(181)	0.448(3)	1.058(2)	1.363(2)	0.1568
C(182)	0.221(3)	1.083(2)	1.396(2)	0.1517
C(191)	0.080(2)	0.867(2)	1.278(2)	0.1226

[a] $U_{eq} = (1/3)\Sigma_i\Sigma_j U_{ij} a_i^* a_j^* a_i a_j$.

linked to Nb(1) (U_{eq} = 0.148 Å^2). However the anisotropic displacement parameter is not completely independent of geometry criteria and in particular the mobility can explain the observed poor bond lengths. The high anisotropic displacement parameter of the carbon C(12) (U_{eq} = 0.198 Å^2) is in agreement with the very short bond length O(12)−C(12) = 1.33 Å. The high mobility of this carbon can explain the particular difficulty in locating its position by Fourier maps.

Solid-State NMR Spectroscopy. Compound **1** has been studied by ^{13}C CP-MAS NMR, including high-power decoupling (see the Experimental Section). The ^{13}C CP-MAS NMR spectrum of compound **1** is shown in Figure 3 and was measured for a contact time t_{CP} = 5 ms. Isotropic chemical shifts are presented in Table 4. The spectrum indicates the presence of three sets of isotropic lines around 25, 75, and 180 ppm. The

Table 2. Selected Bond Distances (Å) for Compound **1**

	First Molecule		
Nb(1)−O(1)	2.18(1)	Nb(1)−O(2)	2.19(1)
Nb(1)−O(3)	1.81(1)	Nb(1)−O(4)	1.87(1)
Nb(1)−O(5)	1.92(1)	Nb(1)−O(6)	1.91(1)
Nb(2)−O(5)	1.86(1)	Nb(2)−O(6)	1.89(1)
Nb(2)−O(7)	1.87(1)	Nb(2)−O(8)	1.89(1)
Nb(2)−O(9)	2.16(1)	Nb(2)−O(10)	2.16(1)
O(1)−C(1)	1.26(2)	O(2)−C(10)	1.27(2)
O(3)−C(3)	1.40(2)	O(4)−C(4)	1.35(3)
O(7)−C(7)	1.36(3)	O(8)−C(8)	1.48(2)
O(9)−C(1)	1.24(2)	O(10)−C(10)	1.24(2)
	Second Molecule		
Nb(3)−O(11)	1.93(1)	Nb(3)−O(12)	1.84(1)
Nb(3)−O(13)	2.18(2)	Nb(3)−O(14)	1.87(1)
Nb(3)−O(15)	2.13(1)	Nb(3)−O(16)	1.90(1)
Nb(4)−O(11)	1.90(1)	Nb(4)−O(16)	1.86(1)
Nb(4)−O(17)	1.89(1)	Nb(4)−O(18)	1.90(1)
Nb(4)−O(19)	2.15(1)	Nb(4)−O(20)	2.20(1)
O(12)−C(12)	1.33(3)	O(13)−C(19)	1.23(2)
O(14)−C(14)	1.44(2)	O(15)−C(15)	1.22(2)
O(17)−C(17)	1.41(3)	O(18)−C(18)	1.45(2)
O(19)−C(19)	1.27(2)	O(20)−C(15)	1.27(2)

Table 3. Selected Bond Angles (deg) for Compound **1**

	First Molecule		
O(1)−Nb(1)−O(2)	83.1(5)	O(1)−Nb(1)−O(3)	82.0(5)
O(2)−Nb(1)−O(3)	80.0(5)	O(1)−Nb(1)−O(4)	176.3(5)
O(2)−Nb(1)−O(4)	93.4(5)	O(3)−Nb(1)−O(4)	98.6(6)
O(1)−Nb(1)−O(5)	86.8(5)	O(2)−Nb(1)−O(5)	169.8(5)
O(3)−Nb(1)−O(5)	99.6(5)	O(4)−Nb(1)−O(5)	96.7(6)
O(1)−Nb(1)−O(6)	81.5(4)	O(2)−Nb(1)−O(6)	81.1(5)
O(3)−Nb(1)−O(6)	156.2(5)	O(4)−Nb(1)−O(6)	96.8(5)
O(5)−Nb(1)−O(6)	96.5(5)	O(5)−Nb(2)−O(6)	93.9(5)
O(5)−Nb(2)−O(7)	99.0(5)	O(6)−Nb(2)−O(7)	94.9(5)
O(5)−Nb(2)−O(8)	99.6(5)	O(6)−Nb(2)−O(8)	159.1(5)
O(7)−Nb(2)−O(8)	98.7(6)	O(5)−Nb(2)−O(9)	87.8(5)
O(6)−Nb(2)−O(9)	83.4(5)	O(7)−Nb(2)−O(9)	173.2(5)
O(8)−Nb(2)−O(9)	81.2(5)	O(5)−Nb(2)−O(10)	169.7(5)
O(6)−Nb(2)−O(10)	82.1(5)	O(7)−Nb(2)−O(10)	90.8(6)
O(8)−Nb(2)−O(10)	82.0(5)	O(9)−Nb(2)−O(10)	82.4(5)
Nb(1)−O(1)−C(1)	137.2(12)	Nb(1)−O(3)−C(3)	144.3(13)
Nb(1)−O(2)−C(10)	136.4(13)	Nb(1)−O(5)−Nb(2)	151.2(6)
Nb(1)−O(4)−C(4)	154.6(24)	Nb(2)−O(7)−C(7)	152.8(19)
Nb(1)−O(6)−Nb(2)	148.5(6)	Nb(1)−O(9)−C(1)	136.0(11)
Nb(2)−O(8)−C(8)	144.5(11)	Nb(2)−O(10)−C(10)	137.9(14)
	Second Molecule		
O(11)−Nb(3)−O(12)	97.4(6)	O(11)−Nb(3)−O(13)	83.3(5)
O(12)−Nb(3)−O(13)	91.5(6)	O(11)−Nb(3)−O(14)	158.8(5)
O(12)−Nb(3)−O(14)	95.7(6)	O(13)−Nb(3)−O(14)	79.7(5)
O(11)−Nb(3)−O(15)	83.5(5)	O(12)−Nb(3)−O(15)	175.6(6)
O(13)−Nb(3)−O(15)	84.3(5)	O(14)−Nb(3)−O(15)	82.2(6)
O(11)−Nb(3)−O(16)	94.0(5)	O(12)−Nb(3)−O(16)	98.0(6)
O(13)−Nb(3)−O(16)	170.5(6)	O(14)−Nb(3)−O(16)	100.6(5)
O(15)−Nb(3)−O(16)	86.3(5)	O(11)−Nb(4)−O(16)	95.7(5)
O(11)−Nb(4)−O(17)	97.0(6)	O(16)−Nb(4)−O(17)	96.7(6)
O(11)−Nb(4)−O(18)	157.9(5)	O(16)−Nb(4)−O(18)	99.2(5)
O(17)−Nb(4)−O(18)	97.4(6)	O(11)−Nb(4)−O(19)	82.9(5)
O(16)−Nb(4)−O(19)	170.2(6)	O(17)−Nb(4)−O(19)	93.1(6)
O(18)−Nb(4)−O(19)	79.6(5)	O(11)−Nb(4)−O(20)	83.0(5)
O(16)−Nb(4)−O(20)	85.3(5)	O(17)−Nb(4)−O(20)	178.0(6)
O(18)−Nb(4)−O(20)	82.0(6)	O(19)−Nb(4)−O(20)	84.9(6)
Nb(3)−O(11)−Nb(4)	145.4(6)	Nb(3)−O(12)−C(12)	158.1(24)
Nb(3)−O(13)−C(19)	134.4(15)	Nb(3)−O(14)−C(14)	145.1(13)
Nb(4)−O(20)−C(15)	130.2(13)	Nb(3)−O(15)−C(15)	133.3(13)
Nb(4)−O(17)−C(17)	144.6(22)	Nb(3)−O(16)−Nb(4)	149.7(7)
Nb(4)−O(19)−C(19)	135.5(15)	Nb(4)−O(18)−C(18)	143.3(13)

first one is assigned to the methyl groups of acetate ligands and isopropoxy groups. The two groups of resonances located at about 74 and 78 ppm of equal intensities correspond to ^{13}CH of isopropoxy groups. These two main distinct resonances are in agreement with the presence of two chemically nonequivalent isopropoxy groups bonded to each niobium atom. One isopropoxy is in an axial position while the other is located in an equatorial position. Each of these main resonances is composed of a set of resonances which strongly overlap, confirming that the environments of these isopropoxy groups are not very

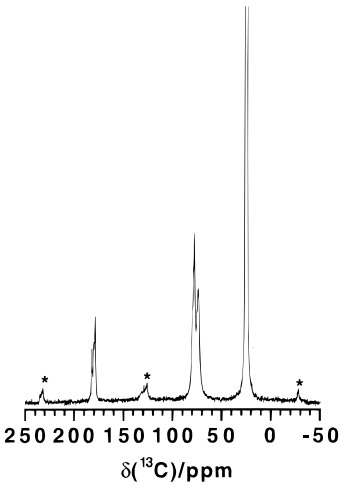

Figure 3. ^{13}C CP MAS NMR spectrum of compound **1** (ν_{rot} (rotation speed) = 4000 Hz; ^{13}C (Larmor frequency) = 75.47 MHz; NS (number of scans) = 600; t_{CP} (contact time) = 5 ms; RD (recycle delay) = 10 s; LB (line broadening) = 20 Hz). (* = spinning sidebands.)

Table 4. Isotropic Chemical Shifts, Line Widths, and Assignments for Compound **1**

δ (ppm)	LW (Hz)	assgnt
24.9	66	*C*H$_3$
25.5	56	*C*H$_3$
26.3	56	*C*H$_3$
73.6	160	*C*H[a]
74.5	145	*C*H
75.6	145	*C*H
78.1	130	*C*H
79.1	150	*C*H
80.2	150	*C*H
178.9	53	*C*OO
179.6	60	*C*OO
180.5	65	*C*OO
182.4	60	*C*OO

[a] Six lines corresponding to CH sites are listed in connection with the IRCP experiments presented below.

different in the structure. The presence of four lines located around 180 ppm characteristic of ^{13}COO$^-$ groups is in agreement with four carboxylato ligands contained in the asymmetric unit. The small chemical shift difference between carboxylate resonances reflects the very close geometry (angles and distances) determined for the COO groups. As the bands around 75 and 180 ppm overlap, it is impossible to assign directly ^{13}C NMR signals to given crystallographic sites.

However, it is well-known that rapid internal molecular motion may lead to partial averaging of NMR interactions, which are anisotropic in nature.[23] These interactions are essentially chemical shift anisotropy (CSA) and dipolar coupling (with ^{1}H) in the case of ^{13}C solid-state NMR spectroscopy. An indirect measurement of the dipolar coupling strength can be obtained by careful analysis of the magnetization transfer between the ^{1}H spin bath and the ^{13}C nuclei during the CP experiment, as this process is strongly related to the dipolar interaction. Any rapid local anisotropic motion will then modulate the dipolar interaction leading to modified CP parameters (see below). Our goal is to correlate the CP behavior of the different nuclei (especially in the CH region) with the anisotropic displacement parameters which are markedly different for the various sites (Table 5). This allows definite assignments to be made. Such a study is usually based on

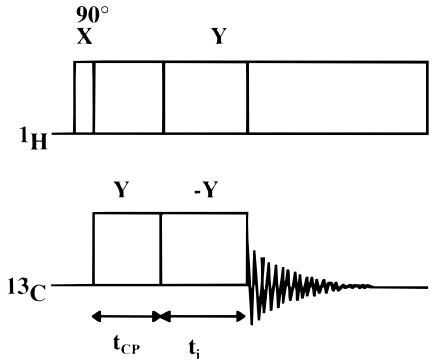

Figure 4. IRCP sequence based upon the standard ^{13}C CP MAS experiment [25] t_{CP} = 5 ms (fixed); t_i = inversion time (variable)).

Table 5. Selected Bond Lengths, Angles, and Anisotropic Displacement Parameters for the Methine CH Carbons of Isopropoxy Groups

C*H	d(O−C*) (Å)	Nb−O−C* (deg)	U_{eq} (Å^2)
C(3)	1.4	144.3	0.082
C(4)	1.35	154.6	0.148
C(7)	1.36	152.8	0.165
C(8)	1.48	144.5	0.096
C(12)	1.33	158.1	0.198
C(14)	1.44	145.1	0.112
C(17)	1.41	144.6	0.155
C(18)	1.45	143.3	0.118

variable contact-time (t_{CP}) experiments, including experiments with very short contact time.[24] However, such an approach suffers from bad signal-to-noise ratios as the contact times used are not sufficient to create significant magnetization. Recently, new techniques based on inversion of polarization, such as IRCP (inversion recovery cross polarization),[25,26] were introduced in the literature for the measurement of dipolar coupling in various organic compounds and inorganic materials.[27−30] It was shown that the dynamics of polarization and inversion of polarization were strictly analogous[31] and that this inversion technique presented the following advantages over variable contact-time experiments: (i) The inversion of polarization occurs after a long contact time thereby enhancing S/N ratio, and subtle CP behaviors can be observed even in the case of strongly overlapping lines.[32] (ii) The inversion of the lines occurs from +1 (in arbitrary units of peak area) to −1, leading to a doubled scale of investigation when compared to standard variable contact-time experiments. Analysis of the results is thus much easier. Moreover, it can be noted that the IRCP technique allows one to perform a total spectral editing of the lines, based on the number of directly bonded protons at each ^{13}C site.[25] In particular, this sequence is effective to differenciate strongly coupled ^{13}C sites such as ^{13}CH and ^{13}CH$_2$ in contrast to the spectral editing sequence NQS (non quaternary supression).[33,34] The IRCP sequence is presented in Figure 4. It is derived from a classic CP sequence. During the relatively long contact time t_{CP}, all the ^{13}C nuclei are polarized. In the second step, a 180° phase shift is operated on the ^{13}C channel. The spin polarization

(23) Mehring, M. *Principles of High-Resolution NMR in Solids*, 2nd ed.; Springer-Verlag: Berlin, 1983; Chapter 2.
(24) Lauprêtre, F.; Monnerie, L.; Virlet, J. *Macromolecules* **1984**, *17*, 1397.
(25) Wu, X.; Zilm, K. W. *J. Magn. Reson.* **1993**, *A102*, 205.
(26) Wu, X.; Burns, S. T.; Zilm, K. W. *J. Magn. Reson.* **1994**, *A111*, 29.
(27) Palmas, P.; Tekely, P.; Canet, D. *J. Magn. Reson.* **1993**, *A104*, 26.
(28) Hirschinger, J.; Hervé, M. *Solid State NMR* **1994**, *3*, 121.
(29) Bonhomme, C.; Maquet, J.; Livage, J.; Mariotto, G. *Inorg. Chim. Acta* **1995**, *230*, 85.
(30) Bonhomme, C.; Tolédano, P.; Maquet, J.; Livage, J.; Bonhomme-Coury, L. *J. Chem. Soc., Dalton Trans.* **1997**, *9*, 1617.
(31) Wu, X.; Zhang, S.; Wu, X. *Phys. Rev. B* **1988**, *37*, 9827.
(32) Babonneau, F.; Maquet, J.; Bonhomme, C.; Richter, R.; Roewer, G. *Chem. Mater.* **1996**, *8*, 1415.

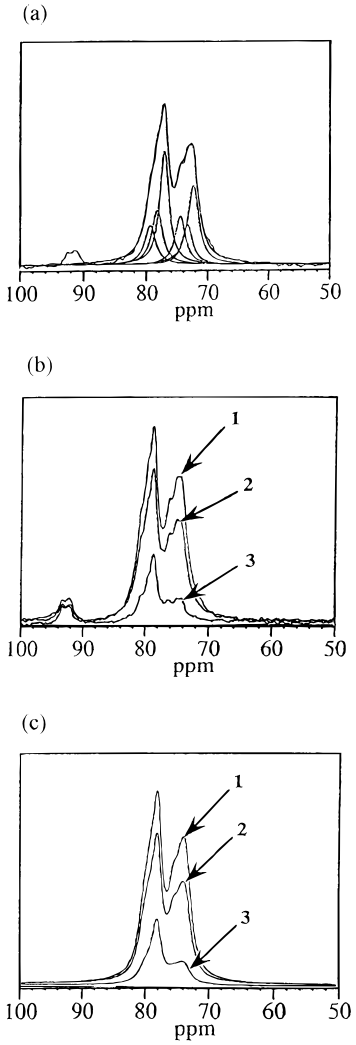

Figure 5. (a) Deconvolution of the CH region (^{13}C CP MAS NMR spectrum of compound **1**). The inversion time is 5 μs (corresponding to the standard CP experiment). (b) Evolution of the CH magnetization as a function of t_i (1, $t_i = 5$ μs; 2, $t_i = 15$ μs; 3, $t_i = 35$ μs). (c) Simulation of the CH region as a function of t_i using the deconvolution presented in (a) (1, $t_i = 5$ μs; 2, $t_i = 15$ μs; 3, $t_i = 35$ μs).

will progressively invert during the inversion time t_i. As this technique is very sensitive to local proton environment, a careful study of the IRCP dynamics allows distinctions to be made between the different CH_x sites. Furthermore, as the $^{13}C-^{1}H$ dipolar coupling is strongly affected by local motion, this sequence reveals information about molecular motion.

The ^{13}C IRCP MAS NMR spectra in the region corresponding to isopropoxy CH sites (δ = 73.6−80.2 ppm) for various inversion times t_i are presented in Figure 5. The spectra obtained for short inversion times are first deconvoluted[35] in order to determine a reasonable number of lines for the fitting procedure. Agreement with experimental data is obtained with six Lorentzian peaks having roughly equivalent line widths (130−160 Hz) (Figure 5a and Table 4). Chemical shifts are located at 73.6, 74.5, 75.6, 78.1, 79.2, and 80.2 ppm. All the IRCP spectra are fitted by using the same set of lines: Chemical shifts, line widths, and line shapes are kept constant; only the amplitudes are allowed to vary (Figure 5b,c). The evolution of each normalized magnetization is then plotted versus t_i (Figure 6) and analyzed by the procedure presented below.

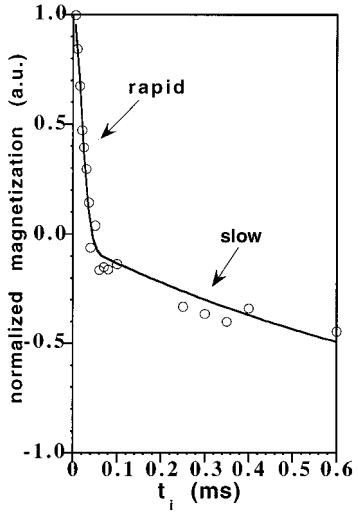

Figure 6. Evolution of the normalized magnetization versus t_i in the IRCP experiment for δ = 73.6 ppm. Two regimes of polarization inversion (rapid and slow) are clearly shown.

In the case of strongly coupled sites such as CH, the expression for the magnetization as a function of inversion time t_i is (neglecting relaxation)[25]

$$M_C(t_i) = M^\circ \left[\frac{2}{n+1} \exp\left(-\frac{t_i}{T_D}\right) + \frac{2n}{n+1} \exp\left(-\frac{3}{2}\frac{t_i}{T_D}\right) \exp\left(-\frac{t_i^2}{T_C^2}\right) - 1 \right] \quad (1)$$

M° denotes the magnetization attained after a contact time t_{CP} and corresponds to the maximum magnetization obtained during the CP process. When a fraction of M° is reached after t_{CP}, eq 1 can be slightly modified. t_i is the inversion time. n corresponds to the number of directly bonded protons in the CH_n groups. T_C is related to the strength of the C−H dipolar coupling between ^{13}C nuclei and directly bonded protons. T_D is a time constant related to the spin diffusion process involving all the remaining protons. This expression shows that the polarization inversion is described by two regimes. This model contrasts with the standard approach of CP involving the monoexponential growth of the magnetization[36] (this model is actually suitable for slightly coupled sites or quaternary ^{13}C). T_C reveals the rapid decrease of the magnetization during the first regime, and T_D is characteristic of the second step where the magnetization decreases slowly ($T_C \ll T_D$). In the case of a rigid CH group T_C is estimated to 25 μs.[29,30] As T_C is an inverse measurement of the dipolar coupling (see eq 1), any reduction of the dipolar coupling by motional averaging will lead to an increase of T_C. This equation also shows that the magnetization is dependent on the n value. Furthermore, as the dynamics of the two regimes are very different, the curve has a turning point which corresponds to the end of the first regime. At this point, the magnetization depends on the value of n and is expressed by the following equation:

$$\left(\frac{1-n}{1+n}\right)M^\circ \quad (2)$$

In the case of CH groups, the turning point is 0. It has been suggested in the literature that the turning point was relatively

(33) Alla, M.; Lippmaa, E. *Chem. Phys. Lett.* **1976**, *37*, 260.
(34) Opella, S. J.; Frey, M. H. *J. Am. Chem. Soc.* **1979**, *101*, 5854.
(35) Massiot, D.; Thiele, H.; Germanus, A. *Bruker Rep.* **1994**, *140*, 43.
(36) Pines, A.; Gibby, M. G.; Waugh, J. S. *J. Chem. Phys.* **1973**, *59*, 569.

Table 6. T_C and T_D Values for the Various CH Lines Involved in the Fitting Procedure[a]

δ (ppm)	T_C (μs)	T_D (ms)	δ (ppm)	T_C (μs)	T_D (ms)
73.6	27	1.0	78.1	42	2.9
74.5	31	1.7	79.1	31	3.6
75.6	28	1.2	80.2	34	2.8

[a] T_D values are approximate as experimental data obtained for high t_i are more dispersed.

Table 7. M° and $T^H_{1\rho}$ Parameters for the Various CH Lines[a]

δ (ppm)	$M°$ (%)	$T^H_{1\rho}$ (ms)
73.6	22	60
74.5	11	29
75.6	12	42
78.1	27	46
79.2	15	30
80.2	13	22

[a] Variable contact-time experiments were performed. Experimental data were analyzed using eq 3.

insensitive to molecular motion.[25] As shown in Figure 6, the evolution of the magnetization for the various lines during the inversion process is clearly characterized by two regimes. The rapid regime occurs during the first tens of microseconds followed by much slower decrease of the magnetization. A turning point at roughly 0 is observed corresponding to the IRCP behavior of a CH group (see above). T_C and T_D parameters are obtained from the eq 1 with $n = 1$ and are listed in Table 6 for all lines involved in the fitting procedure. $T_C \ll T_D$ thereby accounting for the strong coherent transfer of polarization between the ^{13}C nuclei and the directly attached protons. The different lines can be separated in two groups. The first group of lines corresponds to $\delta = 78.1$ and 80.2 ppm with $T_C \geq 34$ μs. These T_C values are much higher than those observed for rigid CH groups. Reduction of the dipolar coupling by molecular motion can be evoked to explain this observation. All other lines are characterized by $T_C \leq 31$ μs corresponding to less reduced dipolar interaction.

To obtain quantitative data for these lines, standard variable contact-time experiments were performed. For the CP experiment, the process again occurs in two stages for strongly coupled ^{13}C sites such as CH, and the increase of magnetization during the contact time is described by the following expression:[25]

$$M_C(t_{CP}) = M°\left[1 - \frac{1}{n+1}\exp\left(-\frac{t_{CP}}{T_D}\right) - \frac{n}{n+1}\exp\left(-\frac{3}{2}\frac{t_{CP}}{T_D}\right)\exp\left(-\frac{t_{CP}^2}{T_C^2}\right)\right]\exp\left(-\frac{t_{CP}}{T^H_{1\rho}}\right) \quad (3)$$

$T^H_{1\rho}$ is the relaxation time of the abundant spins in the rotating frame which is responsible for the decrease of magnetization for long contact time. Data from the ^{13}C CP MAS NMR experiments are analyzed using eq 3. Five parameters should have been fitted (T_C, T_D, n, $T^H_{1\rho}$, $M°$), but three of them (T_C, T_D, n) are already obtained from the IRCP experiments. Therefore, only $T^H_{1\rho}$ and $M°$ are fitted. The extracted parameters are given in Table 7. $M°$ is expressed in relative percent. These values are estimates as the different lines overlap. Nevertheless, it can be assumed that the lines located at $\delta = 78.1$ ppm and $\delta = 73.6$ ppm are twice as intense as the other lines. It follows that the lines located at higher fields ($\delta = 73.6$, 74.5, and 75.6 ppm) correspond roughly to 50% of the total integrated lines in agreement with our previous estimations (vide supra). Lines at lower fields correspond as well to ≈50%. Several assignments related to U_{eq} (see Table 5) can now be proposed.

The lines at 78.1 and 80.2 ppm which correspond to the highest T_C values (Table 6) can be assigned to the C(7), C(12), and C(17) atoms, showing the largest anisotropic displacement parameters. As U_{eq} for C(12) is clearly higher than all other values, C(12) can be safely assigned to $\delta = 78.1$ ppm. The problem is to identify the second carbon since C(7) and C(17) present similar anisotropic displacement parameters (U_{eq}(C(7)) $= 0.165$ Å^2 and U_{eq}(C(17)) $= 0.155$ Å^2). However, C(7) adopts a similar geometry to C(12) since the interatomic distance (O(7)−C(7) = 1.36 Å) and the angle (Nb(2)−O(7)−C(7) = 152.8°) are very close to those found for C(12) (O(12)−C(12) = 1.33 Å, Nb(3)−O(12)−C(12) = 158.1°). The very short bonds O(7)−C(7) and O(12)−C(12) reflect the high mobility of these carbons. The peak at 78.1 ppm can be associated to carbons C(12) and C(7). For C(7) and C(12), the isotropic chemical shifts must be so close that a single resonance is observed ($\delta = 78.1$ ppm). Consequently, the resonance located at 80.2 ppm can be assigned to C(17). The C(3) and C(8) atoms showing the lowest anisotropic displacement parameters can be associated to $\delta = 75.6$ ppm and/or $\delta = 73.6$ ppm. Indeed, these lines are characterized by low T_C parameters corresponding to rigid CH groups. It is difficult to propose definite assignments in this case. It can be noted that the C(3), C(8), C(14), and C(18) atoms are located in axial isopropoxy groups whereas the C(4), C(7), C(12), and C(17) atoms are located in equatorial isopropoxy groups. Considering our previous assignments, the axial ^{13}C are characterized by higher field chemical shifts, whereas the equatorial ^{13}C are characterized by lower field chemical shifts.

Therefore the $\delta = 79.2$ ppm can be safely assigned to C(4). Definite assignments for C(14) and C(18) ($\delta = 74.5$ and 75.6 ppm) cannot be given at the present time.

Careful analysis of the CP process allows one to propose indirect assignment of several of the observed lines. Complete assignment is not possible, but interesting correlations between equatorial/axial ^{13}C, $^{13}C-^{1}H$ dipolar coupling, and isotropic chemical shifts are revealed.

Liquid-State Spectroscopy (Infrared and NMR). Infrared spectra of complex **1** were recorded in CCl_4 solution and in KBr disks (4000−400 cm^{-1}). The complex remains stable in solution since both spectra are identical. The location of the main absorptions bands is presented in the Experimental section.

The ^{17}O NMR spectrum of compound **1** has been recorded in C_6D_6 solution. The ^{17}O nucleus is difficult to observe by NMR spectroscopy for two main reasons. First, it is a spin $I = {}^5/_2$ with an appreciable electric quadrupole moment ($Q = -2.6 \times 10^{-26}$ cm^2) which in general leads to rapid quadrupole relaxation. This rapid relaxation is avantageous in that it allows rapid RF pulsing using the FT NMR technique. However, due to broad resonances a poor spectral resolution and signal-to-noise ratios are obtained. This rapid relaxation requires the use of short delay times between the end of RF pulse and the beginning of data collection. Thus baseline distortions are often observed in transformed spectra. The low natural abundance (0.037%) of ^{17}O nucleus limits observation of its NMR signals. This problem may be overcomed by ^{17}O enrichement. In the sol−gel process, ^{17}O-enriched water is used. The poly(oxo alkoxides) or the oxo polymers which result from the reaction of metal alkoxides with ^{17}O-enriched water are selectively enriched at the oxo bridges.[8] ^{17}O NMR experiments have been carried out for titanium oxo clusters or titanium oxo polymers.[8−10]

In the present study, the niobium isopropoxide is not directly

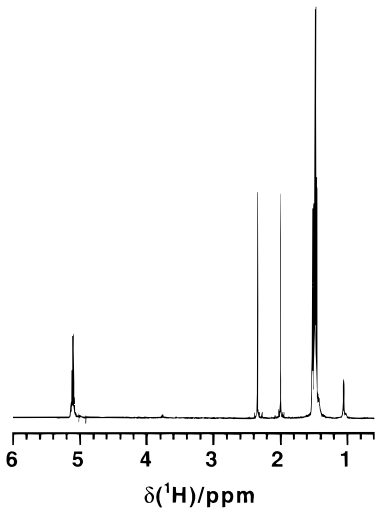

Figure 7. ^{1}H liquid-state NMR spectrum of compound **1**.

Table 8. ^{1}H and ^{13}C NMR Data for Compound **1**

$\delta(^{1}H)$ (ppm)	$\delta(^{13}C)$ (ppm)	J_{H-H} (Hz)	assgnt
1.47, 1.49, 1.52	25.3, 25.4, 25.6	6.2	(CH_3)CH
2.0	24.4		CH_3COO
2.35	24.8		CH_3COO
5.11	79.4	6.2	(CH_3)CH
5.12	74.6	6.2	(CH_3)CH
	180.0		CO
	180.2		CO

hydrolyzed; it was not possible to use ^{17}O-enriched water. Consequently the ^{17}O spectrum was recorded with an extensive signal accumulation (NS = 244 000) in order to obtain a good signal-to-noise ratio. The ^{17}O NMR spectrum of compound **1** displays two resonances at δ = 502 and 529 ppm of equal integrated intensities. ^{17}O NMR studies of polyoxometalates allow assignment of these two peaks to Nb_2O oxygens.[37,38] The lines can be assigned to the two μ_2-oxo oxygens surrounding each niobium atom. Since each $Nb_4O_4(OAc)_4(OPr^i)_8$ cluster contains two Nb_2O oxygens, ^{17}O NMR spectroscopy shows that the molecular structure is preserved in solution. The remaining resonance near 285 ppm is assigned to oxygens of isopropoxy and acetate groups. This peak is particularly broad due either to a distribution of chemical shifts or quadrupole relaxations.

The ^{1}H and ^{13}C NMR spectra were measured in C_6D_6 solution (see Table 8 and Figures 7 and 8). NMR studies performed on oxo alkoxide clusters reveal that it is possible to assign the different signals.[1,17,21] All of the resonances associated with isopropyl groups and acetate ligands are present in ^{1}H and ^{13}C NMR spectra. The ^{1}H NMR spectrum displays three sets of resonances located at about 1.4, 2, and 5.1 ppm (see Table 8). The two signals (δ = 2.00 and 2.35 ppm) with equal intensities can be assigned to the methyl moieties of two nonequivalent acetate groups. The ^{13}C NMR spectrum confirms this observation since it exhibits two distinct resonances corresponding to the methyl of acetate groups (δ = 24.4 and 24.8 ppm).[17,21] However the carbonyl groups C═O have distinct, but quite close, resonances (δ = 180.0 and 180.2 ppm). It seems that the methyl groups experience a higher local field difference probably due to steric hindrance effects.

Two septuplets at 5.10 and 5.12 ppm are partially overlapped and in a 1:1 ratio. The chemical shifts, the multiplicity, and the J couplings ($^{3}J_{H-H}$ = 6.2 Hz) are characteristic of methine isopropoxy protons. The ^{13}C NMR spectrum exhibits two signals (δ = 74.6 and 79.4 ppm) assigned to the methine carbons of isopropoxy groups.[1] This is in agreement with the assignment of ^{13}C resonances of C*H groups proposed for the solid-state ^{13}C NMR spectrum. The two components located at $\delta \approx 79$ and 75 ppm correspond to equatorial terminal isopropoxy groups and axial terminal isopropoxy groups linked to niobium atoms, respectively.

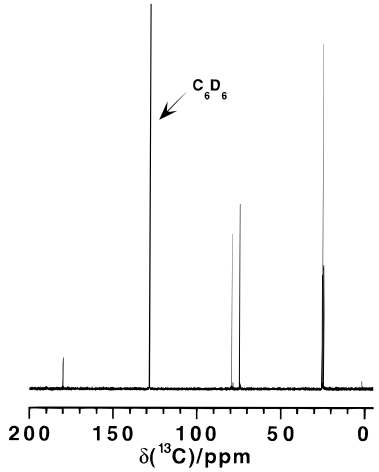

Figure 8. ^{13}C liquid-state NMR spectrum of compound **1**.

^{13}C−^{1}H heteronuclear shift correlated NMR experiments (see Experimental Section) allow better assignment of the resonances corresponding to methine isopropoxy groups and methyl acetate groups. These results are presented in Table 8. The ^{1}H NMR resonance located at δ = 5.10 ppm corresponds to the ^{13}C resonance at 79.4 ppm which was assigned to the equatorial isopropoxy groups. The other septuplet located at 5.12 ppm can be assigned to the proton of the methine carbon of the axial isopropoxy groups. The ^{1}H NMR methyl resonances of the isopropoxy group are characterized by three sets of doublets ($^{3}J_{H-H}$ = 6.2 Hz) located at 1.52, 1.49, and 1.47 ppm with respective intensities of 1:2:1. A direct assignment of these resonances is not possible because of severe overlap.

NMR characterization in solution suggests that only one averaged niobium environment can be observed in solution. Each niobium is surrounded by two μ_2-oxo oxygens which correspond to the two signals at δ = 503 and 529 ppm in the ^{17}O NMR spectrum.

Each niobium atom is also coordinated by two acetate ligands and by two terminal isopropoxy ligands whose corresponding signals are present in the ^{1}H and ^{13}C NMR spectra. It is suggested that the equatorial and the axial terminal isopropoxy groups can be distinguished on the basis of their chemical shifts. The resonances located at lower fields ($\delta \approx 79$ ppm) and higher fields ($\delta \approx 75$ ppm) correspond to equatorial terminal isopropoxy groups and axial terminal isopropoxy groups, respectively.

Proposed Mechanism for the Formation of $Nb_4O_4(OAc)_4(OPr^i)_8$. A general scheme for the proposed mechanism is given in Figure 9. Compound **1** is obtained with a good yield by using a $HOAc/Nb(OPr^i)_5$ ratio of 2. The reaction between the niobium isopropoxide and acetic acid is stoichiometric for a ratio 1/1[39] and can be described as follows:

(37) Filowitz, M.; Ho, R. K. C.; Klemperer, W. G.; Shum, W. *Inorg. Chem.* **1979**, *18*, 93.
(38) Weiner, H.; Aiken, J. D., III; Finke, R. G. *Inorg. Chem.* **1996**, *35*, 7905.
(39) Griesmar, P.; Papin, G.; Sanchez, C.; Livage, J. *Chem. Mater.* **1991**, *3*, 335.

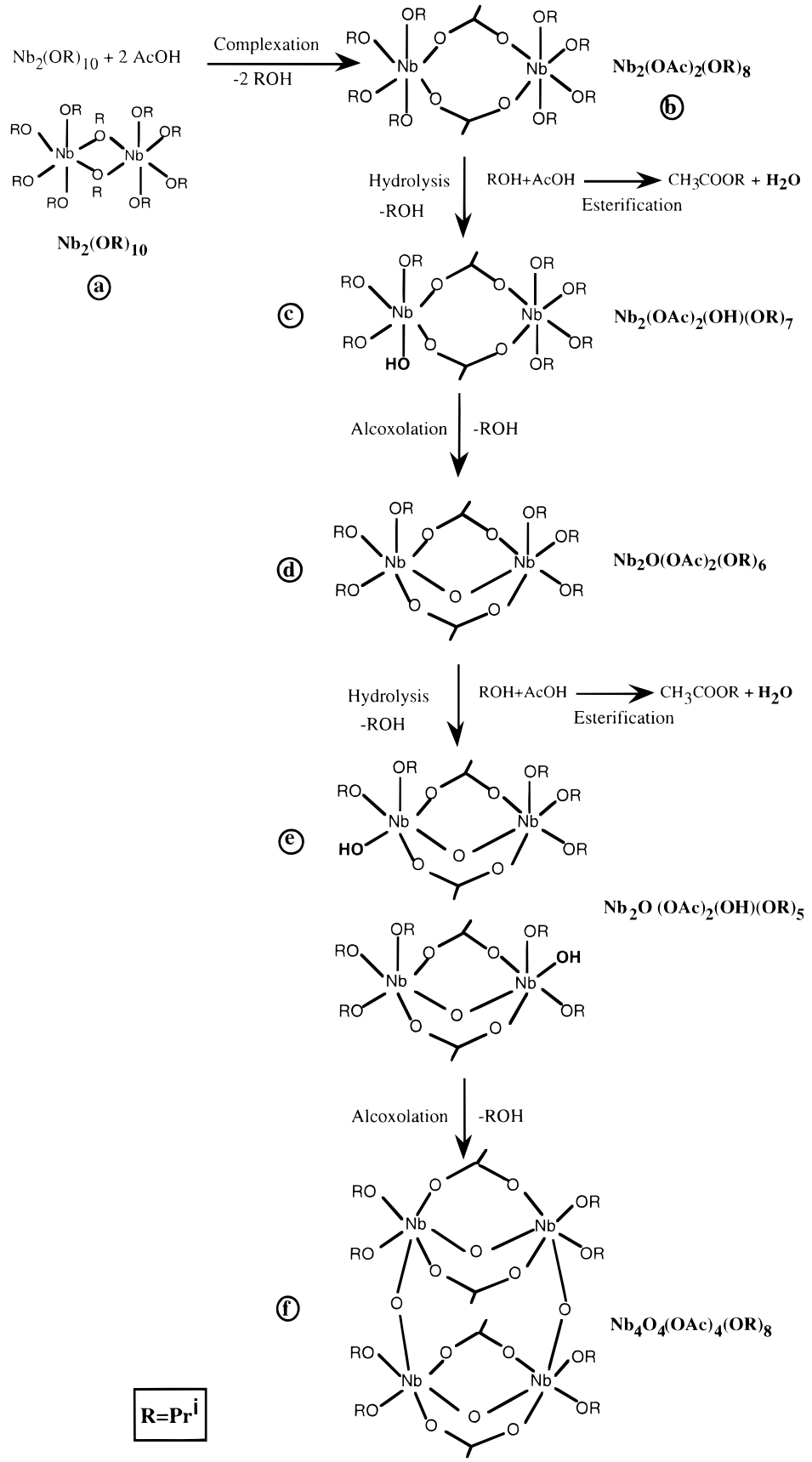

Figure 9. Proposed mechanism for the formation of compound **1**.

$$Nb(OPr^i)_5 + HOAc \rightarrow Nb(OAc)(OPr^i)_4 + HOPr^{i*}$$

The structures of niobium alkoxides and acetic acid modified niobium alkoxides precursors have been investigated by solution ^1H, ^{13}C NMR, and FTIR experiments.[39−42] They correspond to dimers of $Nb_2(OR)_{10}$ and $Nb_2(OAc)_2(OR)_8$ whose structures are schematically shown in Figure 9a,b, respectively. The bridging coordination mode adopted by the carboxylato ligands[39]

contributes to satisfy the 6-fold coordination of the niobium atom. For HOAc/Nb(OPr^i)$_5$ ratios higher than 1, the excess of acid reacts with the 2-propanol (HOPr^{i*}) released in solution leading to ester (isopropyl acetate) and water:

$$HOPr^{i*} + HOAc\ (excess) \rightarrow AcOPr^i + H_2O$$

This reaction was evidenced by infrared spectroscopy. The ester species are characterized by the stretching vibration ν(C=O) = 1740 cm^{-1}, whereas acetate groups bonded to niobium atoms are characterized by two stretching vibrations ν_{sym}(COO) = 1450 cm^{-1} and ν_{asym}(COO) = 1590 cm^{-1}. The in situ generated water probably promotes hydrolysis of some Nb−OPr^i bonds leading to Nb−OH reactive groups. Because the niobium coordination is satisfied in such precursors, condensation occurs through an alcoxolation reaction.[7] Nb−OH groups react readily with other isopropoxy groups present inside the dimeric structure $Nb_2(OAc)_2(OH)(OR)_7$ (Figure 9c) (intermolecular alcoxolation) to form dimers $Nb_2O(OAc)_2(OR)_6$ (Figure 9d). Dimers (Figure 9d) are bonded through μ_2-oxo and carboxylato bridges. ROH groups are preferentially released because they are better leaving groups than acetic acid.[7] The subsequent hydrolysis of $Nb_2O(OAc)_2(OR)_6$ (Figure 9d) leads to $Nb_2O(OAc)_2(OH)(OR)_5$ (Figure 9e). Finally, double alcoxolation between two $Nb_2O(OAc)_2(OH)(OR)_5$ (Figure 9e) entities leads to compound **1** (Figure 9f).

Conclusion

The compound $Nb_4O_4(OAc)_4(OPr^i)_8$ has been characterized by single-crystal X-ray diffraction and multinuclear NMR experiments performed in the solid state and in solution. A simple possible mechanism that can account for its formation is presented. It is demonstrated that ^{13}C CP MAS experiments using the IRCP sequence (inversion recovery cross polarization) can bring indirectly information about ^{13}C assignments. Such analysis can be extended to other clusters containing protonated organic groups. Moreover, ^{17}O, ^{13}C, and ^{1}H NMR spectroscopies reveal that the cluster structure is fully preserved in solution, making this cluster a building block precursor for the synthesis of sol−gel derived materials.

Experimental Section

Synthesis of $Nb_4O_4(OAc)_4(OPr^i)_8$. Nb(OPr^i)$_5$ was synthesized by anodic dissolution of the metal in HOPr^i in the presence of the LiCl and was sublimed at 100 °C and 10^{-1} Torr.[43] The purity was checked by ^{17}O, ^{13}C, and ^{1}H solution NMR spectroscopy. Nb(OPr^i)$_5$ (0.015 mol, 6 g) and acetic acid (purchased from Prolabo) (0.031 mol, 1.76 mL) were stirred until a clear colorless solution was obtained. The reaction mixture was stored for a few days at ambient temperature in a closed vessel. Crystals of $Nb_4O_4(OAc)_4(OPr^i)_8$ (compound **1**) were grown from solution (yield: 62%). IR (KBr) (cm^{-1}): 1450 (ν(COO)$_{sym}$); 1590 (ν(COO)$_{asym}$); 659 (ν(Nb−O)); 2900, 1200, 1000 (ν(CH) and (ν(CO)); 1331, 1371 (δ(C−H)$_{sym}$ and δ(C−H)$_{asym}$). Anal. Found for $Nb_4O_4(OAc)_4(OPr^i)_8$: Nb, 34.6; C, 33.2; H, 5.8; O, 26.2. Calcd: Nb, 32.5; C, 33.6; H, 5.9; O, 28.

Crystallography. All measurements were carried out at room temperature using a Nonius CAD4 diffractometer with Mo Kα radiation (λ = 0.710 69 Å). Details of the crystallographic data collection and structure determinations for the compound **1** are given in Table 9. A suitable crystal (0.1 mm × 0.25 mm × 0.3 mm) was chosen and placed in a glass capillary with silicon oil. Cell dimensions were determined from 25 reflections ($14.5 < \theta < 15°$) dispersed in reciprocal space. The intensities of two standard reflections monitored every 2 h during data collection decayed uniformly. The data were scaled accordingly. The measured intensities were corrected for the effects of Lorenz and polarization. Direct methods using SHELXS-86 programs[44] and successive Fourier maps were used to locate the positions of all non-hydrogen atoms. Full-matrix least-squares refinement of atomic parameters and anisotropic displacement parameters were carried out using CRYSTALS-96 programs.[45] The scattering factors were provided by the *International Tables for X-ray Crystallography*.[46] The H atoms were not located.

Table 9. Crystallographic Data for $Nb_4O_4(OAc)_4(OPr^i)_8$

formula	$Nb_4O_4C_{32}H_{68}$
fw	1144.5
cryst system	triclinic
space group	$P\bar{1}$
a (Å)	11.634(5)
b (Å)	14.370(6)
c (Å)	16.380(6)
α (deg)	79.90(4)
β (deg)	71.78(4)
γ (deg)	79.21(4)
V (Å^3)	2535(35)
Z	2
ρ_{obsd} (g·cm^{-3})	1.5
μ (cm^{-1})	9.04
λ (Å)	0.710 69
temp (°C)	25
decay of std reflcns (%)	50
R^a	0.071
$R_w{}^b$	0.078 ($w = 1$)

^{a} $R = \Sigma||F_o| - |F_c||/\Sigma|F_o|$. ^{b} $R_w = [\Sigma w(|F_o| - |F_c|)^2/\Sigma w|F_o|^2]^{1/2}$.

^{17}O NMR Spectroscopy of $Nb_4O_4(OAc)_4(OPr^i)_8$. The ^{17}O NMR spectra were recorded at 54.2 MHz on a Bruker MSL 400 spectrometer. A 90° pulse was used and recycle delay was 0.2 s. A delay of 36 μs (DW = 6 μs) was set before signal acquisition. All experiments were carried out under argon in a glovebox in order to avoid hydrolysis. Crystals of $Nb_4O_4(OAc)_4(OPr^i)_8$ (0.5 g, 0.437 mmol) were dissolved in 2.5 mL of benzene, and the solution was transferred to an NMR tube. ^{17}O NMR (C_6D_6, 22 °C) [δ (assignment, number of oxygen atoms, $\Delta\nu_{1/2}$ in Hz)]: 529 (Nb_2−O, 2 O, 100 Hz), 502 (Nb_2−O, 2 O, 54 Hz), 285 (Nb−OPr^i, 8 O, 4600 Hz).

^{1}H and ^{13}C NMR Spectroscopy of $Nb_4O_4(OAc)_4(OPr^i)_8$. The ^{1}H and ^{13}C NMR experiments (1D and 2D ^{1}H−^{13}C) were performed on a Bruker AC 500 spectrometer (500.13 MHz for ^{1}H and 125.76 MHz for ^{13}C). All experiments were carried out under argon in a glovebox in order to prevent hydrolysis with atmospheric water. Crystals of $Nb_4O_4(OAc)_4(OPr^i)_8$ (0.25 g, 0.218 mmol) were dissolved in 300 μL of perdeuterated benzene, and the solution was transferred to an NMR tube. Chemical shifts are referenced to TMS.

^{1}H NMR (C_6D_6, 22 °C) [δ (number of H, multiplicity, J, assignment)]: 1.47, 1.49, 1.52 (48, d, $^3J_{H-H}$ = 6.1 Hz, CH_3 in OPr^i); 2.00 (6, s, CH_3 in OAc); 2.35 (6, s, CH_3 in OAc); 5.10, 5.12 (8, sept, $^3J_{H-H}$ = 6.1 Hz, CH in OPr^i).

^{13}C NMR (C_6D_6, 22 °C) [δ (assignment)]: 24.4, 24.8 (CH_3 in OAc); 25.3, 25.4, 25.6 (CH_3 in OPr^i); 74.6, 79.4 (CH in OPr^i); 180.0, 180.2 (CO in OAc).

The 2D ^{1}H−^{13}C COSY NMR experiment was detected in reverse mode (^{1}H) using the Bruker INVDR2D2 microprogram.[47]

^{13}C Solid-State NMR Spectroscopy of $Nb_4O_4(OAc)_4(OPr^i)_8$. The spectra were recorded at room temperature on a Bruker MSL 300 spectrometer at 75.47 MHz for ^{13}C (^{1}H, 300.13 MHz) with a Bruker

(40) Pfalzgraf, L. G.; Riess, J. G. *Bull. Soc. Chim. Fr.* **1968**, 4348.
(41) Pfalzgraf, L. G.; Riess, J. G. *Bull. Soc. Chim. Fr.* **1973**, 1201.
(42) Bradley, D. C.; Holloway, C. E. *J. Chem. Soc. A* **1968**, 219.
(43) Yanovskii, A. I.; Turevskaya, E. P.; Turova, N. Y.; Dolgushin, F. M.; Pisarevskii, A. P.; Batsanov, A. S.; Struchov, Y. T. *Russ. J. Inorg. Chem.* **1994**, *39*, 1307.
(44) Sheldrick, G. M. *SHELXS-86*, *Program for crystal structure solution*; University of Göttingen: Göttingen, Germany, 1986.
(45) Watkins, D. J.; Prout, C. K.; Carruthers, R. J.; Betteridge, P. W. *Crystals-96 Issue 10*; Chemical Crystallography Laboratory, University of Oxford: Oxford, U.K., 1996.
(46) *International Tables for X-ray Crystallography*; Kynoch Press: Birmingham, England, 1974; Vol. IV.
(47) Bax, A.; Giffery, R. H.; Hawkins, B. L. *J. Magn. Reson.* **1983**, *55*, 301.

CP MAS probe using 7 mm ZrO_2 rotors. The rotors were filled with freshly synthesized ground crystals. As the crystals are moisture sensitive, all experiments were carried out under argon atmosphere in a glovebox. Rotors were spun at 4000 ± 2 Hz, allowing the suppression of CSA for CH_3 and CH sites. All the CP and IRCP experiments were performed under the same Hartmann−Hahn match condition, which was carefully set and periodically checked ($t_{90°}(^1H) = 6\ \mu s$). Isotropic chemical shifts are referenced to TMS. The ^{13}C CP MAS NMR spectra were recorded with 20 different contact times t_{CP} up to 15 ms. The IRCP experiments were performed with $t_{CP} = 5$ ms and with 20 inversion times varying from 5 μs to 1 ms. The recycle delay between pulses was 10 s. The number of scans was 600 and 904 for each CP and IRCP experiment, respectively. The spectra were simulated with the WIN-FIT program.[35]

Supporting Information Available: Tables S1−S4, listing atomic coordinates, anisotropic thermal parameters, and complete bond lengths and angles (4 pages). Ordering information is given on any current masthead page.

IC971024I